Open access • Proceedings Article • DOI:10.1109/CEIT.2016.7929055

Oil spill segmentation in fused Synthetic Aperture Radar images

Fodio S Longman, Lyudmila Mihaylova, Daniel Coca

Institutions: University of Sheffield

Published on: 01 Dec 2016 - International Conference on Control, Engineering & Information Technology

Topics: Synthetic aperture radar

Proceedings Paper:
Longman, F.S., Mihaylova, L.S. orcid.org/0000-0001-5856-2223 and Coca, D. (2017) Oil Spill Segmentation in Fused Synthetic Aperture Radar Images. In: 2016 4th International Conference on Control Engineering & Information Technology (CEIT). 4th International Conference on Control Engineering & Information Technology, 16-18 Dec 2016, Hammamet, Tunisia. IEEE . ISBN 978-1-5090-1055-4

https://doi.org/10.1109/CEIT.2016.7929055

Oil Spill Segmentation in Fused Synthetic Aperture Radar Images

Fodio S Longman , Lyudmila Mihaylova and Daniel Coca
Department of Automatic Control and System Engineering,
University of Sheffield, Mappin Street, S1 3JD, UK
Email: fslongman1@sheffield.ac.uk*, l.s.mihaylova@sheffield.ac.uk and d.coca@sheffield.ac.uk

***Abstract*—Synthetic Aperture Radar (SAR) satellite systems are very efficient in oil spill monitoring due to their capability to operate under all weather conditions. Systems such as the Envisat and RADARSAT have been used independently in many studies to detect oil spill. This paper presents an automatic feature based image registration and fusion algorithm for oil spill monitoring using SAR images. A range of metrics are used to evaluate the performance of the algorithm and to demonstrate the benefits of fusing SAR images of different modalities. The proposed framework has shown 45% improvement of the oil spill location when compared with the individual images before the fusion.**

Keywords: Oil Spill, Synthetic Aperture Radar (SAR), Registration, Image Fusion, Segmentation

I. Introduction

Remote sensing systems offer the advantage of being able to observe events in remote and mostly inaccessible areas through images. They also provide wide area coverage of these events. A single remotely sensed image from a satellite system has the capability of covering hundreds of kilometres of earth surface. Thanks to such advantages, remote sensing data (images) from satellite systems are used extensively in the monitoring of different disasters on earth.

Oil is vital in our daily life activities. Products from oil such as petrol and gas are used both industrially and domestically. This requires transporting oil between countries and continents on sea across the world. During this transportation, oil spill can happen. Oil spill from vessels, offshore oil platforms and oil pipelines severely pollute marine and coastal habitats causing enormous damage to the natural environment and great loss to the economy. One such oil spill is that of the Deep Water Horizon (also referred to as Gulf of Mexico Oil Spill, BP Oil Disaster and the Macondo Blowout) [1], as a result of the explosion and sinking of the Deep Water Horizon oil rig on the 20th April 2010, causing the sea floor oil gusher to flow for 87 days resulting in the loss of lives and damage to the marine ecosystems.

Synthetic Aperture Radar (SAR) images are ideal for monitoring oil spills as they are not affected by local weather conditions and cloudiness [2]. Oil spills appear as dark areas on SAR images [3]. However, the ability of radar to detect oil is limited by sea conditions. Low sea state conditions (1-3 on Douglas scale [4]) will not produce enough sea clutter in the surrounding sea to contrast with the oil and very high sea conditions (7-9 on Douglas scale [4]) will scatter radar sufficiently to block detection inside the wave troughs [5]. Despite this, SAR images represent a fundamental tool in the detection and monitoring of oil spill [6].

SAR systems such as the Canadian RADARSAT and Envisat satellite of the European Space Agency (ESA) operating in different bands and imaging mechanisms have been used independently to detect and monitor oil spill.

In this paper, an image fusion algorithm of SAR images for oil spill monitoring is proposed. The aim is to obtain an image of higher quality than the individual images. Image Fusion is a subset of the more diverse research area data fusion [7]. It provides a framework and tools that align data originating from different sources with the aim of obtaining information of greater quality depending on the type of application [8]. The fusion of SAR images, however, poses several problems such as registration, due to multi-modality, differences in imaging mechanisms between the sensors and choosing a suitable fusion method to bring the complimentary and supplementary information together.

This paper proposes an algorithm for automatic feature based registration and fusion of SAR images containing oil spill which combines data acquired from different sensors using RADARSAT-2 and Envisat images [9] of the Gulf of Mexico Oil Spill scene acquired on the 26th and 29th of April 2010 respectively. The paper is organised as follows. In section II, the registration process is explained. Section III presents the image fusion approach based on the discrete wavelet transform (DWT). Section IV introduces the metrics used to evaluate the quality of the fused images and Section V summarises the result.

A. Proposed Framework of SAR Image Fusion

The proposed framework of SAR image fusion is shown in Fig 1. It comprises a preprocessing step followed by automatic feature based image registration and fusion. SAR images contain speckle noise and often have a poor visualisation. The preprocessing step helps to manage this noise by filtering the images and also improves the visualisation by an enhancement to obtain the best possible image perception. A Gaussian filter, which preserves edges, texture and fine details of the image is used to reduce the effect of speckle noise and improve the image quality. The registration step and the fusion methods will be explained in subsequent sections of the paper.

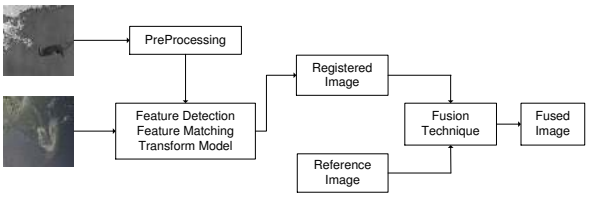

Fig. 1: SAR Image Fusion Framework

II. Image Registration

Image registration is a crucial step in image fusion since the final information is gained from the combination of various data sources [10]. It is the process of mapping similarity between two images of the same scene that are taken at different times, from different viewpoints, and or by different sensors [11]. In remote sensing, registration is required to perform tasks such as environmental monitoring, change detection, weather forecasting and creating super-resolution images to mention a few. The goal is to establish the correspondence between two different images and determine the geometric transformation that aligns one image with the other [12].

In this paper, the registration is done automatically using the scale-invariant feature transform (SIFT) algorithm. Proposed in [13], the SIFT algorithm extracts distinctive invariant features from images that are used to perform reliable matching between different views of an object or scene of an image. Features in an image include edges, area and points [11]. The SIFT features are invariant to scale, rotation, affine distortion and noise which makes them often more effective and robust than other features [14]. The SIFT algorithm involve four steps that are summarised below.

A. Scale Space Extrema Detection

The scale-space extrema is a function $L(x,y,\sigma)$, it is the product of convolution of the variable scale Gaussian kernel $G(x,y,\sigma)$ with the image $I(x,y)$.

$$L(x, y, \sigma) = G(x, y, \sigma) * I(x, y) \tag{1}$$

where $*$ is the convolution operator with respect to x and y pixel coordinates, σ is the standard deviation, $I(x, y)$ is the image with spatial co-ordinates x and y and

$$G(x, y, \sigma) = \frac{1}{2\pi\sigma^2} e^{-\frac{x^2+y^2}{2\sigma^2}} \tag{2}$$

is the Gaussian filter. To detect features, [13] and [11] proposed using scale-space extrema in the Difference-of-Gaussian (DoG) function convolved with the image, such that:

$$\begin{aligned} D(x, y, \sigma) &= (G(x, y, k\sigma) - G(x, y, \sigma)) * I(x, y) \\ &= L(x, y, k\sigma) - L(x, y, \sigma) \end{aligned} \tag{3}$$

where k is the multiplicative factor usually set to $\sqrt{2}$ [13] [14]. To detect the local maxima and minima of $D(x,y,\sigma)$, each sample point is compared to its eight neighbours in the current image and nine neighbours in the scale and below.

B. Keypoint Localisation

Once keypoints are found by comparing a pixel to its neighbours, the next step involves fitting it to a nearby data for location, scale and rotation [13]. The purpose of this step is to remove noise-sensitive points or non-edge points to enhance stability of the matching process and improve immunity to noise [11]. In [13], it is proposed that the extreme points of low contrast is removed by expanding the scale space function using the Taylor series such that:

$$D = (x, y, \sigma). \tag{4}$$

C. Orientation Assignment

In orientation assignment, the location information is extracted from the keypoints with identified location and scale. The orientation assignment describes the feature point location information based on the local characteristics of the image. This will often make the feature descriptors remain invariant to rotation by forming the orientation histogram from gradient orientations of the neighbouring pixels of the keypoints. Based on the orientation histogram, the keypoints are then assigned.

Let L be the Gaussian smoothed image to which the scale of the keypoint is selected with the closest scale, so that all computations are performed in a scale-invariant manner. For each image sample $L(x,y)$ at that scale, the magnitude of the gradient $m(x,y)$, and the orientation $\theta(x,y)$, are precomputed using the pixel differences as illustrated in [13].

D. Keypoint Descriptor

This phase computes the descriptor for the local image region which is highly distinctive and yet as invariant as possible to other variations such as illumination and angle of view change. The keypoint descriptor is created by first computing the magnitude of gradients and orientation at each image sample point in the region within the keypoint location as illustrated in the left side of Fig. 2. This region is weighted by a Gaussian window as indicated by the overlaid circle. Secondly, the samples are added to form orientation histograms summarising the contents over an 8×8 subregions as shown on the right hand side of Fig. 2, with the length of each arrow corresponding to the sum of the magnitude gradients near that direction within the region. The histograms are integrated into a vector of fixed length and finally the vector is normalised so that it is invariant to illumination changes and this becomes the SIFT descriptor [14]. Fig. 2 below shows a 2×2 descriptor array computed from 8×8 set of samples. In this paper, we adopt the 4×4 descriptors computed from a 16×16 sample array as shown in [13].

E. Feature Keypoints Matching

The matching step is to find correspondences between the feature points. The best candidate match for each keypoint is found by identifying its nearest neighbour in the database of the keypoints from the extraction step [13]. To discard features without an adequate corresponding match, the distance of the closest neighbour pixel to that of the second closest neighbour

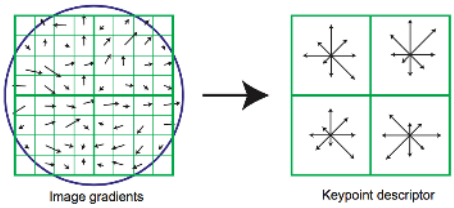

Fig. 2: Keypoint Descriptor [13]

pixel is compared so that correct matches have the closest neighbour matches. However, this may result in many features from one image not having any correct match in the other image and for this reason the RANSAC algorithm [15] is proposed to reject all error matches so that only tentative matches are retained.

F. RANSAC

The random sample consensus algorithm is a robust transformation estimation algorithm [15]. It can handle mapping features in the presence of outliers. It has been proven to work for robust estimation of mapping functions in automatic feature based image registration [16], by finding the homography of each image pair to be registered. In this paper, the RANSAC algorithm is used to find tentative matching feature points from the SAR images and identifies the inliers while eliminating the outliers. To achieve this, a data set M is created which forms the matched points consisting of N data points and then an affine transformation model (H) is established between the feature points. Once this is done, a subset $s1$ of four matched feature points are randomly selected and then H is computed by means of the selected feature points. Let the images to be registered be $I1(x, y)$ and $I2(x, y)$, the model for the affine transformation between them is given by

$$\begin{pmatrix} x_2 \\ y_2 \end{pmatrix} = s \begin{pmatrix} \cos\theta & -\sin\theta \\ \sin\theta & \cos\theta \end{pmatrix} \begin{pmatrix} x_1 \\ y_1 \end{pmatrix} + \begin{pmatrix} t_x \\ t_y \end{pmatrix} \quad (5)$$

where(x_1, y_1) and (x_2, y_2) are the control points coordinates in $I1(x, y)$ and $I2(x, y)$ being the reference and sensed images, respectively. The variables t_x and t_y are the translational values in x and y direction, S is the scaling factor and θ is the angle of rotation.

III. Image Fusion

Fusion of images aims at bringing the complementary information between different imaging sensors together while also enhancing the supplementary information between them [17]. This can be performed at various information levels, such as pixel, feature and decision levels. Several fusion methods have been proposed in the literature for different applications. In the fusion of SAR images, consideration is given to the differences in the characteristics of the imaging sensor since SAR images are formed from the backscattering process of microwave interaction with ground features resulting in images that are relatively rich in higher frequencies in the frequency spectrum. For this reason, [8] suggested that fusion techniques based on frequencies have the advantage to bring the information together per the nature of the images. In this paper, simple average and discrete wavelet transform (DWT) image fusion methods are used to fuse images from RADARSAT-2 and Envisat of the Gulf of Mexico oil spill scene. The simple averaging method to put all pixels in focus and the Discrete Wavelet Transform to check the frequency discrepancy effect between the SAR images.

A. Simple Averaging

The simple average fusion method obtains an output image $I_F(x, y)$ from two input images $I1(x, y)$ and $I2(x, y)$ by taking the average of each pixel value of the input images. This is given as

$$I_F(x, y) = \frac{I1(i, j) + I2(i, j)}{2} \quad (6)$$

where $I_F(x, y)$ is the fused image, $I1(x, y)$ is the registered image, $I2(x, y)$ is the reference image, x and y are the spatial coordinates of the images and the variables i and j represent the pixel values in $I1$ and $I2$.

B. Discrete Wavelet Transform (DWT)

The DWT-based fusion technique is used for image fusion as it improves the spatial resolution of the fused image while preserving the colour appearance for interpretation and further analysis [18]. In the case of oil spill application, preserving the colour appearance is critical as oil is assumed to appear as dark spot on SAR images. The wavelet approach to image fusion allows the image decomposition into different coefficients while preserving the information in the image. This is achieved by converting the image from spatial to frequency domain in such a way that the wavelet filters are applied on a down-sampled image separately in the vertical and horizontal directions. Given an input image $I(x; y)$, the image is filtered by a low pass filter L in the vertical direction and a high pass filter H in the horizontal direction. The image is then down-sampled by the factor of two to retain the alternative sample and to create the coefficient matrices $I_L(x; y)$ and $I_H(x; y)$. The filtered and down-sampled coefficients create sub-bands or sub-images $I_{LL}(x, y)$, $I_{LH}(x, y)$, $I_{HL}(x, y)$, $I_{HH}(x, y)$ [19].

The $I_{LL}(x, y)$ sub image contains the approximation coefficients, $I_{LH}(x, y)$ the horizontal detail coefficients, $I_{HL}(x, y)$ the vertical detail coefficients and $I_{HH}(x, y)$ the diagonal coefficients. The wavelet transform can be performed on multi levels. The next level of decomposition is done only on the sub-image $I_{LL}(x, y)$ resulting in four sub-bands or images with each having the size half of $I_{LL}(x, y)$. This process can be repeated until the desired frequency is attained.

In this paper, $I_1(x, y)$ and $I_2(x, y)$ denote the source images (the co-registered SAR image and the reference image to be fused), the DWT method is then used to decompose them into approximation and detailed coefficients as described above. The DWT and coefficients are combined using a fusion rule

Φ. The fused image $I_F(x, y)$ is obtained by taking the inverse DWT (IDWT) [19].

$$I_F(x, y) = IDWT[\Phi DWT(I_1(x, y), DWT(I_2(x, y))] \quad (7)$$

This process is illustrated in Fig 3. The four level DWT method for fusion of the images is tested and the results obtained are compared with the simple average method.

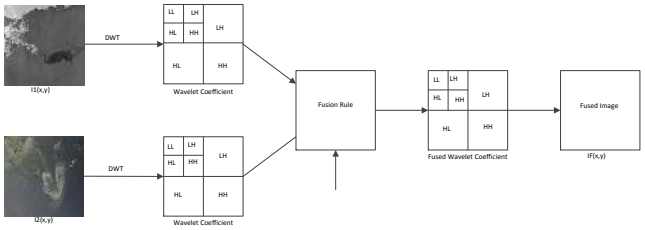

Fig. 3: Wavelet based Image Fusion

IV. Fusion Quality Performance Measures

It is important to evaluate the quality of the fused image using established quality assessment measures. In the literature, several of such quality assessment measures have been defined to determine the quality of fused images and the similarity between individual images fused and the fused image. In [20], the test of quality measure in pan sharpened images was based on the Wald's Protocol where the paradigm is based on two properties; consistency and synthesis. However, quality measures are generally classified into three categories that depend on the aim of the fusion which could be to measure the spatial, spectral or global quality of the fused image. In this paper, the following global quality performance measures are used to test the quality of the fused image.

1. Image Correlation Coefficient (CC): The CC measures the relationship between the fused image and the reference image. The higher the correlation between the fused image and the reference image, the better the estimation of the spectral values [21]. It is also the factor which characterises the geometric distortion between the fused and the reference images [22]. The ideal value for cross correlation is between -1 and 1. Thus, the CC is given as:

$$CC(I1, I2) = \frac{\sum_{mn}(I1_{mn} - \bar{I1})(I2_{mn} - \bar{I2})}{(\sum_{mn}(I1 - \bar{I1}))^2(\sum_{mn}(I1 - \bar{I1}))^2} \quad (8)$$

where $I1_{mn}$ represents one pixel of the fused image of size $(m \times n)$, $\bar{I1}$ is the mean of the fused image. similarly, $I2_{mn}$ represents one pixel of the reference image of size $(m \times n)$ with mean $\bar{I2}$.

2. Spectral Angle Mapper (SAM): The Spectral Angle Mapper computes the spectral angle between the pixel, vector of the reference image and the fused image [23]. SAM is calculated in either degrees or radians and performed on a pixel to pixel basis. The optimal value of SAM is 0. It is defined as

$$SAM(I1, I2) = \frac{1}{n}\sum_{j=1}^{n} SAM(i1_j, i2_j) \quad (9)$$

$$SAM(I1_{\{i\}}, I2_{\{i\}}) = arccos\left(\frac{\langle I1_{\{i\}}, I2_{\{i\}}\rangle}{\|I1_{\{i\}}\| \, \|I2_{\{i\}}\|}\right) \quad (10)$$

where $i1_j$ and $i2_j$ are the jth columns of $I1$ and $I2$ which are the fused and reference image, $\langle I1_{\{i\}}, I2_{\{i\}}\rangle$ are the inner product of the reference and the fused image and $||.||$ is the norm, respectively.

3. Root Mean Squared Error (RMSE): The RMSE measures the difference between the reference and the fused image [24]. It is defined as

$$RMSE = \left(\frac{\sum_{i=1}^{M}\sum_{j=1}^{N}[I2(i, j) - I1(i, j)]^2)}{M \times N}\right) \quad (11)$$

where $I1(i, j)$ and $I2(i, j)$ are the image pixel values for the fused and the reference image, respectively and $M \times N$ is the size of the image.

V. EXPERIMENTAL RESULTS

A. Dataset

The dataset used in this paper are real life SAR images of the oil spill in the Gulf of Mexico from Envisat ASAR instrument and RADARSAT-2 ScanSAR instrument on board ESA's Envisat and Canadian RADARSAT-2 satellites, respectively. In table 1, the dataset is described.

TABLE I: Characteristics of the Dataset:

Satellite	Instrument	Resolution	Band	Dimension	Date Acquired
Radarsat-2	SAR	$100m \times 100m$	C	865×905	29/04/10
Envisat	ASAR	$150m \times 150m$	C	930×1271	26/04/10

The RADARSAT-2 SAR image is a ScanSAR wide single beam mode acquired on April 26th,2010. The ScanSAR mode provides images with very wide swaths in a single pass of the satellite [25]. The original size of the SAR image is 865×905 with a spatial resolution of $100m \times 100m$. The satellite operates in C band. The Envisat image from the ASAR instrument on board ESA's Envisat Satellite is of size 930×1271 with a spatial resolution of $150m \times 150m$ in the wide scan mode and it also operates in the C-band. Both images represent the Gulf of Mexico oil spill scene and were acquired on the 26th and 29th of April 2010, respectively.

B. Results and Discussion

Image enhancement and speckle noise reduction methods discussed in Section I are applied to the SAR images. The registration algorithm described in Section II was applied to both images to align the two images together and match common features between them. The RANSAC is used to remove false matches and retain only tentative ones. The fusion methods described in Section III are applied to the

registered image and the RADARSAT-2 image is used as the reference image to fuse the two images together. The quality measures described in Section IV are used to test the global quality of the fused images. Lastly, the dark spot which is the assumed oil spill position is segmented from the image.

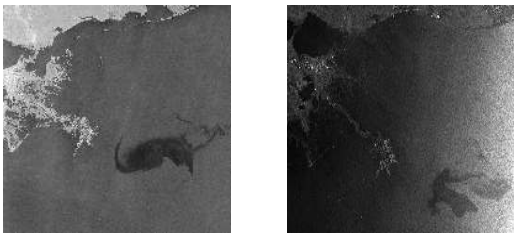

(a) (b)

Fig. 4: RADARSAT-2 ScanSAR and Envisat ASAR images of Gulf of Mexico Oil Spill captured 29/04/2010 and 26/04/2010, respectively.

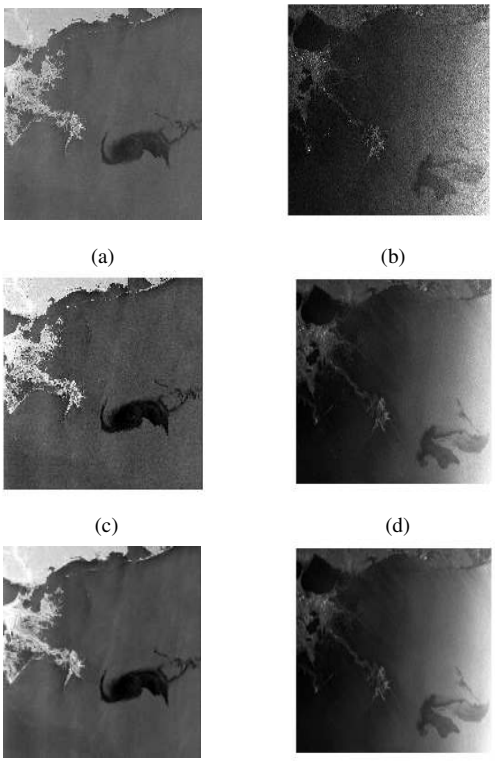

(a) (b)

(c) (d)

(e) (f)

Fig. 5: Pre-Processing of SAR Image (a) Gray Scale ScanSAR (b) Gray ScaleASAR (c) Adjusted ScanSAR (d) Adjusted ASAR (e) and (f) De-noised ASAR and ScanSAR images using a Gaussian filter

The quality metrics discussed in Section IV are used to evaluate the performance of the fusion methods on the fused images. First the CC values obtained are within the ideal value range of -1 and 1, the SAM values are also in considerable range. It is also noticeable that the RMSE values change with the increase in the wavelet decomposition level.

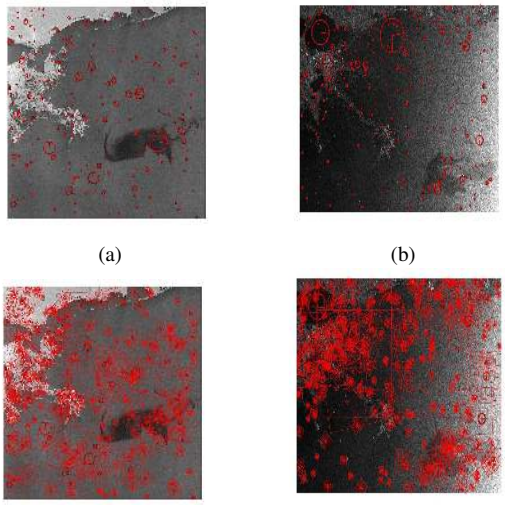

(a) (b)

(c) (d)

Fig. 6: Feature Extraction:(a) and (b) SIFT Features of ScanSAR and ASAR, (c) and (d) SIFT Features with Descriptors

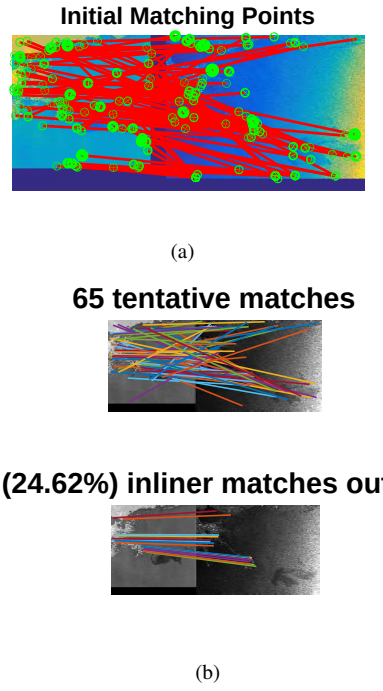

(a)

(b)

Fig. 7: Matching: (a) Initial Matching of Features with 87 points, (b.top) RANSAC tentative matches 65 points, (b.bottom) Inliner Matches 16 representing 26.42% points

VI. Conclusions

This paper demonstrates the potential of automatic feature based image registration and fusion using simple averaging and discrete wavelet transform at different levels on SAR images for the application of oil spill monitoring. The registration and fusion have shown significant improvement in the coverage area of the spill scene when compared to the individual SAR images before fusion. This is useful in monitoring, and

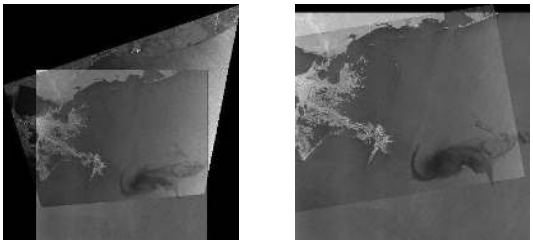

(a) (b)

Fig. 8: (a) Registered Image (b) Fused Image with Simple Average Method

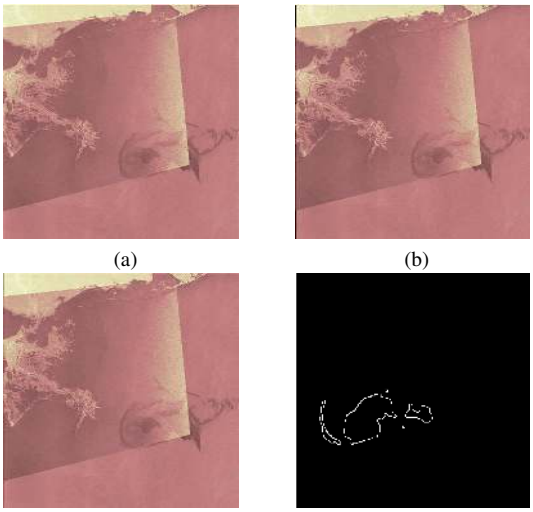

(a) (b) (c) (d)

Fig. 9: DWT Fusion (a) level 1 (b) level 2 (c) level 3 (d) Segmented Dark Spot

TABLE II: Quality Measures of the Fusion Result

Fusion Method	CC	RMSE	SAM
Simple Averaging	0.1274	0.3764	0.003144
DWT Level1	0.2306	0.3609	11.3992
DWT Level2	0.2416	0.3600	11.3822
DWT Level3	0.2384	0.3603	11.3950
DWT Level4	0.2387	0.3603	11.4005

for further image based analysis, including for classification.

ACKNOWLEDGMENT

The authors would like to acknowledge Petroleum Trust Development Fund (PTDF) Nigeria, for funding this work. We will also like to thank the European Space Agency and the Canadian Space Agency for the SAR images used in this work.

REFERENCES

[1] D. H. S. Group, "Final report on the investigation of the macondo well blowout," *Center for Catastrophic Risk Management, University of California at Berkeley*, 2011.

[2] M. Cococcioni, L. Corucci, and B. Lazzerini, "Issues and preliminary results in oil spill detection using optical remotely sensed images," in *Proceedings of OCEANS 2009-EUROPE*, 2009.

[3] A. Sheta, M. Alkasassbeh, M. Braik, and H. A. Ayyash, "Detection of oil spills in sar images using threshold segmentation algorithms," *International Journal of Computer Applications*, vol. 57, no. 7, 2012.

[4] B. C. Douglas, "Global sea level rise," *Journal of Geophysical Research: Oceans*, vol. 96, no. C4, pp. 6981–6992, 1991.

[5] M. Fingas and C. Brown, "Review of oil spill remote sensing," *Marine Pollution Bulletin*, vol. 83, no. 1, pp. 9–23, 2014.

[6] M. Migliaccio, "Synthetic Aperture Radar for oil spill monitoring: a brief review," *in Proceedings of Anais XVII Brazilian Symposium on Remote Sensing*, 2015.

[7] V. R. Pandit and R. Bhiwani, "Image fusion in remote sensing applications: A review," *International Journal of Computer Applications*, vol. 120, no. 10, 2015.

[8] R. Chandrakanth, J. Saibaba, G. Varadan, P. A.-D. Raj *et al.*, "Fusion of high resolution satellite SAR and optical images," in *Proceedings of 2011 International Workshop on Multi-Platform/Multi-Sensor Remote Sensing and Mapping (M2RSM)*. IEEE, 2011, pp. 1–6.

[9] A. H. Solberg, C. Brekke, and P. O. Husoy, "Oil spill detection in Radarsat and Envisat SAR images," *IEEE Transactions on Geoscience and Remote Sensing*, vol. 45, no. 3, pp. 746–755, 2007.

[10] B. Zitova and J. Flusser, "Image registration methods: a survey," *Image and Vision Computing*, vol. 21, no. 11, pp. 977–1000, 2003.

[11] M. Subramanyam and Mahesh, "Automatic feature based image registration using SIFT algorithm," in *Proceedings of 2012 Third International Conference on Computing Communication & Networking Technologies (ICCCNT)*. IEEE, 2012, pp. 1–5.

[12] W. Jia, J. Zhang, and J. Yang, "SAR image and optical image registration based on contour and similarity measures," *Proc. GSEM*, 2009.

[13] D. G. Lowe, "Distinctive image features from scale-invariant keypoints," *International Journal of Computer Vision*, vol. 60, no. 2, pp. 91–110, 2004.

[14] R. Chen, M. Hawes, L. Mihaylova, J. Xiao, and W. Liu, "Vehicle logo recognition by Spatial-SIFT combined with logistic regression," *in Proceedings of the International Conference on Information Fusion 2016*, 2016.

[15] M. Subramanyam and Mahesh, "Automatic feature based image registration using SIFT algorithm," in *Proceedings of 2012 Third International Conference on Computing Communication & Networking Technologies (ICCCNT)*. IEEE, 2012, pp. 1–5.

[16] L.-R. Dung, C.-M. Huang, and Y.-Y. Wu, "Implementation of RANSAC algorithm for feature-based image registration," *Journal of Computer and Communications*, vol. 1, no. 06, p. 46, 2013.

[17] L. Dabbiru, S. Samiappan, R. A. Nobrega, J. A. Aanstoos, N. H. Younan, and R. J. Moorhead, "Fusion of synthetic aperture radar and hyperspectral imagery to detect impacts of oil spill in Gulf of Mexico," in *Proceedings of the 2015 International Geoscience and Remote Sensing Symposium (IGARSS),*. IEEE, 2015, pp. 1901–1904.

[18] M. Berbar, S. Gaber, and N. Ismail, "Image fusion using multi-decomposition levels of discrete wavelet transform," in *Proceedings of International Conference on Visual Information Engineering, 2003. VIE 2003.* IET, 2003, pp. 294–297.

[19] V. Naidu and J. Raol, "Pixel-level image fusion using wavelets and principal component analysis," *Defence Science Journal*, vol. 58, no. 3, p. 338, 2008.

[20] L. Loncan, S. Fabre, L. B. Almeida, J. M. Bioucas-Dias, W. Liao, X. Briottet, G. A. Licciardi, J. Chanussot, M. Simoes, N. Dobigeon *et al.*, "Hyperspectral pansharpening: a review," *IEEE Geoscience and Remote Sensing Magazine*, vol. 3, no. 3, pp. 27–46, 2015.

[21] M. F. Yakhdani and A. Azizi, "Quality assessment of image fusion techniques for multisensor high resolution satellite images (case study: IRS-P5 and IRS-P6 satellite images)," *in Proceedings of the ISPRS TC VII Symposium-100 years ISPRS*, 2010.

[22] L. Loncan, S. Fabre, L. B. Almeida, J. M. Bioucas-Dias, W. Liao, X. Briottet, G. A. Licciardi, J. Chanussot, M. Simoes, N. Dobigeon *et al.*, "Hyperspectral pansharpening: a review," *IEEE Geoscience and Remote Sensing Magazine*, vol. 3, no. 3, pp. 27–46, 2015.

[23] P. Jagalingam and A. V. Hegde, "A review of quality metrics for fused image," *Aquatic Procedia*, vol. 4, pp. 133–142, 2015.

[24] V. R. Pandit and R. Bhiwani, "Image fusion in remote sensing applications: A review," *International Journal of Computer Applications*, vol. 120, no. 10, 2015.

[25] M. Marghany, "Automatic detection of oil spills in the gulf of mexico from RADARSAT-2 SAR satellite data," *Environmental Earth Sciences*, vol. 74, no. 7, pp. 5935–5947, 2015.